Membrane-based processes: optimization of hydrogen separation by minimization of power, membrane area, and cost

Patricia L. Mores [1,†], Ana M. Arias [1,†], Nicolás J. Scenna [1], José A. Caballero [2], Sergio F. Mussati [3], and Miguel C. Mussati [3,*]

[1] CAIMI Centro de Aplicaciones Informáticas y Modelado en Ingeniería, Universidad Tecnológica Nacional, Facultad Regional Rosario, Zeballos 1346, S2000BQA Rosario, Argentina
[2] Department of Chemical Engineering, University of Alicante, Apartado de correos 99, 03080 Alicante, Spain
[3] INGAR Instituto de Desarrollo y Diseño (CONICET−UTN), Avellaneda 3657, S3002GJC Santa Fe, Argentina
[†] The authors have contributed equally.
[*] Correspondence: mmussati@santafe-conicet.gov.ar; Tel.: +54-342-453-4451

Received: date; Accepted: date; Published: date

Abstract: This paper deals with the optimization of two-stage membrane systems for H_2 separation from a $CO_2/CO/H_2/N_2$ gas mixture in order to attain high values of both H_2 recovery and H_2 product purity simultaneously at the minimum total annual cost. For a given H_2 recovery level of 90%, cost optimizations are performed and discussed for desired H_2 product purity values ranging between 0.90 and 0.95 mole fraction. The results showed that the minimal total annual cost increases exponentially with increasing H_2 product purity levels, and that the contribution of the operating expenditures is more significant than the contribution of the annualized capital expenditures (approximately 62% and 38%, respectively). This percentage contribution remains almost constant in the studied range of H_2 product purity values. In addition, the optimal designs (process-units sizes and operating conditions) obtained for different H_2 product purity levels and 90% H_2 recovery are discussed in detail. It was found an increment of H_2 product purity in 0.01 determines different percentage variations in costs depending on the purity level itself. For instance, an increment of H_2 purity from 0.90 to 0.91 implies an increase of the total annual cost in 0.03739 M\$ $yr.^{-1}$ (2.1%) while the same increment from 0.94 to 0.95 implies an increase in 0.17274 M\$ $yr.^{-1}$ (8.4%). Similarly, the optimal trade-offs existing between process variables −like the total membrane area and the total electric power− depend on the specified H_2 product purity level. Finally, the influence of two other single objective functions on the optimal designs of the studied membrane process is analyzed: minimization of the total membrane area and minimization of the total power. For the same design specifications (H_2 recovery of 90% and H_2 product purity of 0.90), a minimal total annual cost of 1.76421 M\$ is obtained by cost minimization, which is about 4.7% and 16.7% lower than the value obtained by minimization of the total membrane area and the total electric power, respectively. From a comparison of the optimization results obtained for the three objective functions, a strategy to systematically and rationally provide `good´ lower and upper bounds for model variables and initial guess values to solve the cost minimization problem by means of global optimization algorithms is proposed, which can be straightforward applied to other processes. From the process system engineering perspective, the proposed optimization model constitutes a valuable decision-support tool to design, simulate, and optimize two-stage membrane processes for hydrogen separation, as well as to elucidate the exiting techno-economic trade-offs that are difficult to distinguish at first glance.

Keywords: H_2 separation; membranes; multi-stage process; optimization; design; operation; cost; membrane area; energy; mathematical programming; NLP; GAMS.

1. Introduction

Together with material science, the mathematical modeling and algorithmic optimization of both the membrane module and the whole membrane-based process are of main concern for improving the performance of this separation technology. Certainly, they can be easily used for testing and providing valuable information about the sizes of the process units as well as the operating conditions of the entire process flow sheet in a short time [1,2].

Depending on the degrees of freedom of the system −the difference between the number of model variables and the number of equality constraints− a mathematical model of the process can be used for two purposes: a) process simulation, when the degrees of freedom is null, and b) process optimization, when the degrees of freedom is higher than 1. In literature, several authors have addressed the optimization of membrane-based processes in several applications by employing simulation-based optimization procedures [1,3−6] and other ones by using rigorous optimization algorithms [7−10]. Without pretending to be an exhaustive review of the state-of-the-art of the types of models and solution strategies −and independently of the membrane materials, geometry and flow pattern, and the processed gas mixtures− some articles are briefly mentioned next that have contributed to membrane separation from the process engineering or process system engineering perspectives. For instance, Xu et al. [3] studied the potential applications of membrane-based processes for hydrogen purification and pre-combustion CO_2 capture. They investigated single-stage and two-stage configurations, and two membrane types: CO_2 selective membranes and H_2 selective membranes (HSMs). Among other results, the authors found that a minimum cost selectivity can be obtained by fixing the membrane permeability along with the H_2 product purity level. Another important result indicated that it is difficult to reach a stable operation mode of the two-stage system with HSM because it is strongly influenced by the variation of the operating conditions. The authors highlighted the need of further investigation in this matter.

Giordano et al. [4] studied a single-stage unit to capture the CO_2 generated in a coal-fired power plant. They investigated the influence of the membrane operating temperature on the CO_2 capture considering two membrane materials with different gas separation properties (permeability and selectivity). Also, the authors considered feed compression and permeate vacuum pumping. Results showed that the increase in the operating temperature determines a decrease in the permeate CO_2 purity and an increase in the electric power requirement.

Ahmad et al. [1] implemented in Aspen HYSYS a two-dimensional mathematical model of a membrane-based process to study the sweetening of natural gas by capturing CO_2. They investigated several design configurations, from single to multiple stages including recycle streams and considering cross-flow pattern. The minimum gas processing cost was obtained with a two-stage membrane configuration where the retentate obtained in the first stage is fed to the second stage and the permeate obtained in the second stage is sent back to the first one.

By using a nonlinear mathematical programming (NLP) model −implemented in GAMS software−, Zarca et al. [7] evaluated a two-stage membrane process for H_2 recovery from the tail gas generated in carbon black manufacturing process, considering two types of membranes: polymeric membranes and ionic liquid-based membranes. Results show that ionic liquid-based membranes are promising not only to achieve a H_2-rich syngas stream at a minimal cost but also to mitigate CO_2 emissions.

Ohs et al. [10] proposed a mixed-integer nonlinear mathematical programming (MINLP) model to address the optimal membrane cascade for N_2 removal from natural gas. As a result, the optimal process configuration with the corresponding membrane areas, pressures of the feed and permeate streams, including the selection of candidate recycle streams, were obtained. They considered CH_4-selective membranes only, N_2-selective membranes only, and combinations of both. They found that about 40% of the cost can be saved if a combination of CH_4 and N_2-selective membranes is used.

This work focuses on the rigorous optimization of membrane-based processes to separate H_2 from a $CO_2/CO/H_2/N_2$ gas mixture generated in hydrocarbons processing plants to attain desired H_2 recovery and product purity levels by minimization of cost, membrane area, and energy, separately. To this end, three NLP problems are solved using the algebraic equation-oriented optimization tool GAMS.

The paper is organized as follows. Section 2 describes the studied two-stage membrane process configuration for hydrogen separation. Section 3 states the optimization problem to be solved. Section 4 summarizes the main model assumptions and considerations and presents the mathematical model employed in this research. Section 5 discusses the optimization results obtained for different H_2 purity target levels and compares the optimal solutions obtained considering different objective functions in the optimization problem. Finally, Section 6 draws the conclusions of this work.

2. Process description

As illustrated in Fig. 1, besides the two membrane units MS1 and MS2, which are the `core´ of the studied separation process, the other main pieces of equipment are the compressors C1 and C2; heat exchangers HEX1, HEX2, and HEX3; vacuum pumps VP1 and VP2; mixers M1 and M2; and splitters SP1 and SP2. The incoming gas mixture feed F_0 increases its pressure in C1 and reaches the operating temperature T_{MS1} in HEX1. Then, it is optionally mixed in M1 with a fraction of the retentate stream obtained in MS1 (RR_{MS1}) and/or a fraction of the retentate obtained in MS2 (RR_{MS2_MS1}). Afterward, the resulting stream is fed to MS1 obtaining two streams: the permeate stream (which is enriched in H_2) and the retentate stream. The permeate membrane side operates under vacuum whether a vacuum pump VP1 is used to create the driving force for component separation. The permeate stream P_{MS1} leaving the VP1 decreases its temperature in HEX2 and increases its pressure in C2. Afterward, it reaches the operating temperature T_{MS2} in HEX3 and can be optionally mixed in M2 with a fraction of the retentate obtained in MS2 (RR_{MS2}). Finally, the resulting stream is fed to MS2 obtaining the retentate and permeate streams corresponding to this stage.

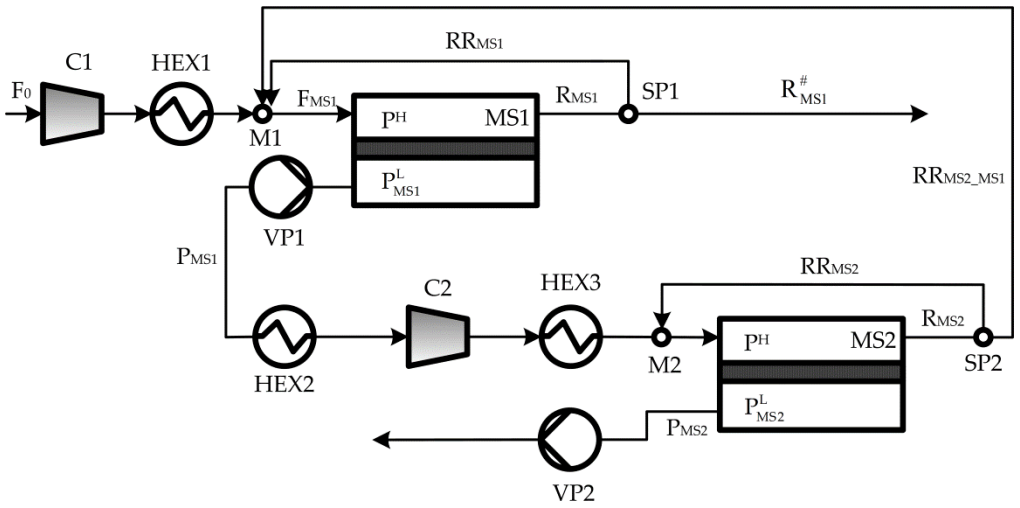

Figure 1. Schematic of the studied two-stage membrane process configuration.

The driving force for component permeation can be created in different ways: (i) by compressing the feed F_0 by means of C1 in the first stage and compressing the permeate P_{MS1} by means of C2 in the second stage (i.e. no vacuum is applied at the permeate side of the membranes); (ii) by applying vacuum at the permeate sides (i.e. no compression of the feed and permeate streams is applied); and (iii) by combining both compression and vacuum. But the best way to create the driving force depends on other factors such as membrane areas, costs, and design specifications. The higher compressor pressure ratio the smaller membrane area and the higher H_2 purity, but the higher power requirement to run the compressor. Similarly, the higher pressure ratio of a vacuum pump the smaller membrane area and the higher H_2 purity, but the higher vacuum level to run the vacuum pump. In both cases, the optimal operating pressure values depend on the relationships between investment and operating costs. Thus, it is clear the importance of optimizing simultaneously all the techno-economic trade-offs that exist between the process variables.

3. Problem statement

The problem stated in this work is the optimal separation of H_2 from a given $CO_2/CO/H_2/N_2$ gas mixture by means of the two-stage membrane process described above, to attain an H_2 recovery target level of 90% varying parametrically the H_2 product purity between 0.90 and 0.95, by minimization of the total annual cost, based on a NLP formulation. Both the permeability and selectivity of the membrane material are assumed to be known and are taken from the literature [7].

As a result, the minimum total annual cost, the optimal process-unit sizes (membrane unit areas, heat exchanger areas, compressor and vacuum-pump power capacities), the optimal operating conditions (pressure, temperature, flow rate, and composition of the retentate and permeate streams), as well as the optimal values of the cost components (total investment, individual process-unit acquisition cost, capital and operating expenditures, among others), are provided.

4. Process modeling

4.1. Assumptions and process mathematical model

Briefly, some main assumptions considered for modeling the membrane unit are the following: the permeability values correspond to the pure species and are not influenced by the operating pressure; steady state behavior; plug-flow pattern; constant total pressure at each membrane side. Regarding the mathematical modeling, the component mass balance in the membrane module is described by a set of algebraic equations obtained by discretization of the resulting set of ordinary differential equations employing the backward finite difference method (BFDM). The mathematical model that describes the process flow sheet illustrated in Fig. 1 involves nonlinear constraints due to the presence of bilinear terms in the mass and energy balances (multiplications of concentrations and flow rates, and multiplications of enthalpies and flow rates) as well as equations to calculate costs. A complete list of the assumptions and the mathematical model used in this study to describe the membrane stages and the other process units (compressors, heat exchangers, etc.) can be found in Arias [11] and Arias et al. [8] and are also provided in Appendix A. Next, the considered cost model is presented.

4.2. Cost model

The total annual cost (TAC, in M\$ $yr.^{-1}$), capital expenditures (CAPEX, in M\$), annualized capital expenditures (annCAPEX, in M\$ $yr.^{-1}$), and operating expenditures (OPEX, in M\$ $yr.^{-1}$) are calculated by Eqs. (1−5).

$$TAC = annCAPEX + OPEX \tag{1}$$

$$annCAPEX = CRF \cdot CAPEX \tag{2}$$

$$CRF = \frac{i \cdot (1+i)^n}{(1+i)^n - 1} \tag{3}$$

$$CAPEX = f_1 \cdot C_{INV} \tag{4}$$

$$OPEX = f_2 \cdot C_{INV} + f_3 \cdot OLM + f_4 \cdot C_{RM} \tag{5}$$

In Eq. (5), OLM accounts for manpower and maintenance costs. A detailed calculation of the economic factors f_1 (4.98), f_2 (0.464), f_3 (2.45), and f_4 (1.055) can be found in [8], which were estimated based on the guidelines given in [12] and [13].

The total investment cost (C_{INV}, in M\$) is calculated by Eq. (6), where the investment costs of the individual process units are estimated by Eqs. (7−10):

$$C_{INV} = I_{C1} + I_{C2} + I_{VP1} + I_{VP2} + I_{HEX1} + I_{HEX2} + I_{HEX3} + I_{MS1} + I_{MS2} \quad (6)$$

$$I_{HEX} = 0.3574 \cdot \left(\frac{A_{HEX}}{929} \right)^{0.6} ; \text{ HEX: HEX1, HEX2, HEX3} \quad (7)$$

$$I_{C} = 2.7878 \cdot \left(\frac{W_{C}}{2000} \right)^{0.6} ; \text{ C: C1, C2} \quad (8)$$

$$I_{VP} = 2.25034\ 10^{-6} \cdot W_{VP}; \text{ VP: VP1, VP2} \quad (9)$$

$$I_{MS} = 5.28034\ 10^{-5} \cdot A_{MS} + 0.24884 \cdot \left(\frac{0.1}{55} \cdot P^{H} \right)^{0.875} \cdot \left(\frac{A_{MS}}{2000} \right)^{0.7} ; \text{ MS: MS1, MS2} \quad (10)$$

The raw material and utility cost (C_{RM}, in M\$ yr.$^{-1}$) used in Eq. (5) is calculated by Eq. (11). It depends on the cost of electricity (C_{EP}), cooling water (C_{CW}), and membrane replacement (C_{MR}), which are expressed by Eqs. (12−14), respectively:

$$C_{RM} = C_{EP} + C_{CW} + C_{MR} \quad (11)$$

$$C_{EP} = cru_{EP} \cdot TW \cdot OT \quad (12)$$

$$C_{CW} = cru_{CW} \cdot F_{CW} \cdot 1.8 \times 10^{-2} \cdot (3600 \cdot OT) \quad (13)$$

$$C_{MR} = 0.2 \cdot cru_{MR} \cdot (A_{MS1} + A_{MS2}) \quad (14)$$

where the specific costs cru_{EP}, cru_{cw}, and cru_{MR} are, respectively, 0.072 \$ kW^{-1}, 0.050929 \$ kg^{-1}, and 10.0 \$ m^{-2}. An operation period (OT) of 6570 h yr.$^{-1}$ was considered.

The complete model describing the entire process contains 3952 equations (equality and inequality constraints) and 3274 variables. It was implemented in GAMS −General Algebraic Modeling System− [14] and solved with CONOPT which is based on the generalized reduced gradient algorithm [15]. Therefore, global optimality of the discussed solutions cannot be guaranteed because of the use of a local search NLP solver. To guarantee it, a global optimization algorithm must be used instead.

5. Results and discussion

The values of the model parameters used are taken from [7], which are listed in Table 1. In Subsection 5.1, optimal solutions obtained by minimizing the total annual cost for a variation range of H_2 product purity are discussed. In Subsection 5.2, optimal solutions obtained by minimizing the total membrane area and the electric power are presented and compared to the obtained by minimizing the total annual cost for the same design specifications.

5.1. Optimal solutions corresponding to the minimization of the total annual cost

The main optimization results for a H_2 recovery target level of 90% and H_2 product purity target values in the range 0.90−0.95are presented in Figs. 2−10.

Table 1. Numerical values of model parameters [7].

Parameter	Value

Feed specification	
Flow rate, mol s^{-1}	0.02777
Temperature, K	313.15
Pressure, MPa	0.10132
Composition (mole fraction)	
CO_2	0.04
CO	0.16
H_2	0.18
N_2	0.62
Membrane material (Polymer)	
Permeance, mole m^{-2} s^{-1} MPa^{-1})	
CO_2	8.4441 10^{-3}
CO	7.4571 10^{-4}
H_2	2.8710 10^{-2}
N_2	4.0781 10^{-4}

Figure 2a shows that the total annual cost (TAC) value increases as the H_2 purity increases since the H_2 permeate flow rate in the first stage increases to satisfy the increased purity, as shown in Figs. 7–9 for H_2 product purity levels of 0.90, 0.91, and 0.94, respectively. For instance, compared to 0.90 H_2 product purity, the minimum TAC value obtained for 0.95 H_2 purity increases by 26.2%, −from 1.76421 to 2.22688 M$ $yr.^{-1}$− as consequence of the increase of both the OPEX value by 25.1% −from 1.09542 to 1.37026 M$ $yr.^{-1}$− and the annCAPEX value by 28.1% −from 0.66879 to 0.85663 M$ $yr.^{-1}$−. On the other hand, it can be observed in Fig. 2b that the contribution ratio between OPEX and annCAPEX to the TAC remains almost constant with increasing H_2 purity values. Certainly, the contribution of OPEX to the TAC varies slightly from 62.1% to 61.6% for H_2 product purity values of 0.90 and 0.95, respectively.

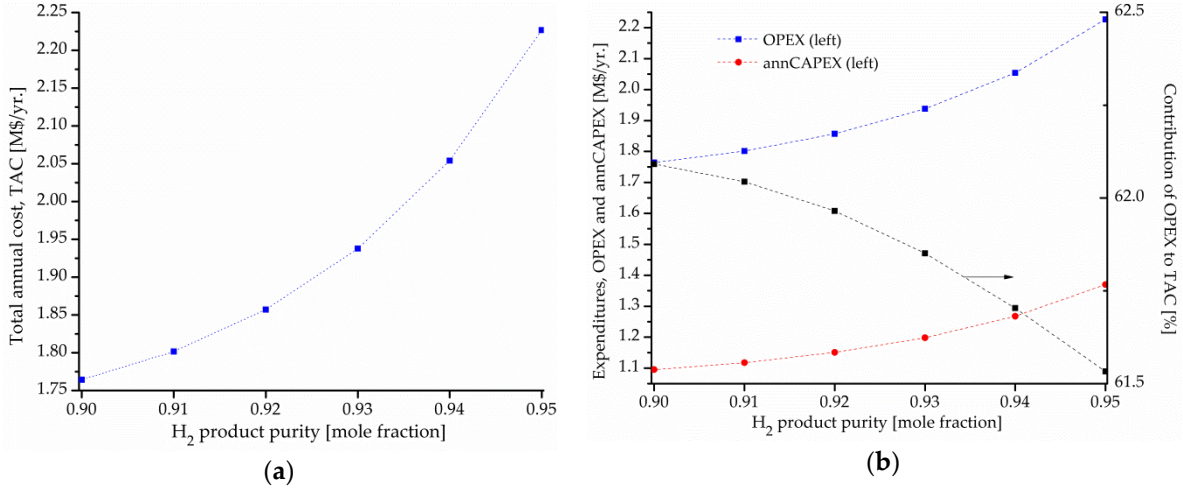

Figure 2. TAC minimization. Optimal costs vs. H_2 product purity for a H_2 recovery of 90%: (**a**) TAC; (**b**) OPEX, annCAPEX, and percentage contribution of OPEX to TAC.

Also, Fig. 2a shows that an increment of H_2 product purity in 0.01 determines different percentage variations in costs depending on the purity level itself. For instance, an increment of H_2 purity from 0.90 to 0.91 implies an increase of TAC in 0.03739 M$ $yr.^{-1}$ (from 1.76421 to 1.80160 M$ $yr.^{-1}$, i.e. 2.1%) while the same increment from 0.94 to 0.95 implies an increase of TAC in 0.17274 M$ $yr.^{-1}$ (from 2.05414 to 2.22688 M$ $yr.^{-1}$, i.e. 8.4%).

By comparing Figs. 3 and 4 it can be observed that an increment of H_2 purity from 0.90 to 0.94 increases the permeate flow rate −from 0.008 to 0.013 kmol s^{-1}− and H_2 concentration −from 0.710 to

0.774 mole fraction− in the first stage, but decreases the permeate flow rate in the second stage −from 4.986x10^{-3} to 4.774x10^{-3} kmol s^{-1}−. It is interesting to note that, in order to reach these flow rate values and H_2 purities, the electric power requirement by compressors and vacuum pump increases in total 0.108 MW (0.026 MW, 0.049 MW, and 0.033 MW in C1, C2, and VP1, respectively) while the optimal total membrane area decreases 332.1 m^2 (58.0 m^2 and 274.1 m^2 in the first and second stage, respectively). Thus, the optimal cost-based trade-offs indicate that it is more beneficial to increase the total electrical power −to operate the process at higher operating pressure values P^H as shown in Fig. 5− rather than to increase the total membrane area.

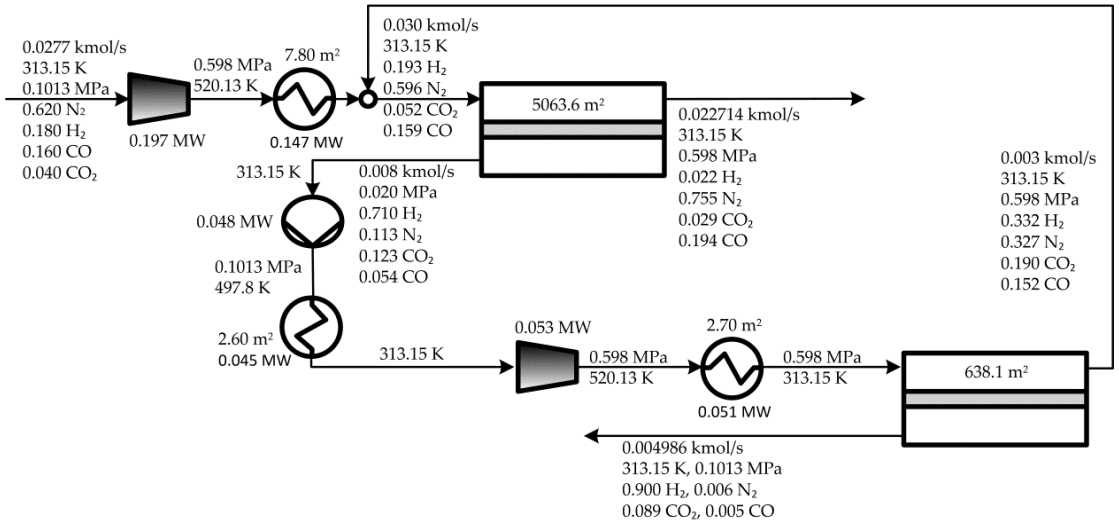

Figure 3. TAC minimization. Optimal solution for a H_2 product purity of 0.90 and H_2 recovery of 90%

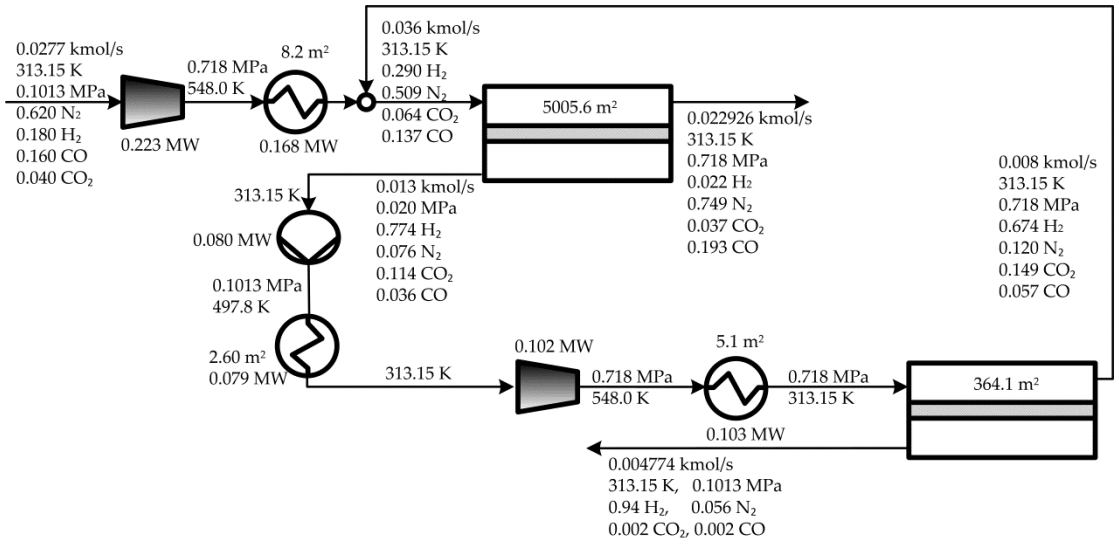

Figure 4. TAC minimization. Optimal solution for a H_2 product purity of 0.94 and H_2 recovery of 90%

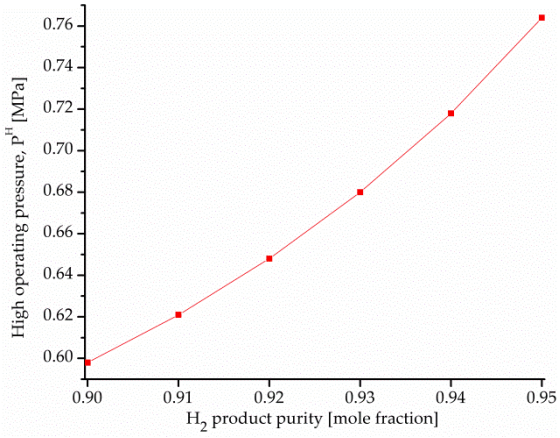

Figure 5. TAC minimization. Optimal high operating pressure P^H (retentate side) versus H_2 product purity.

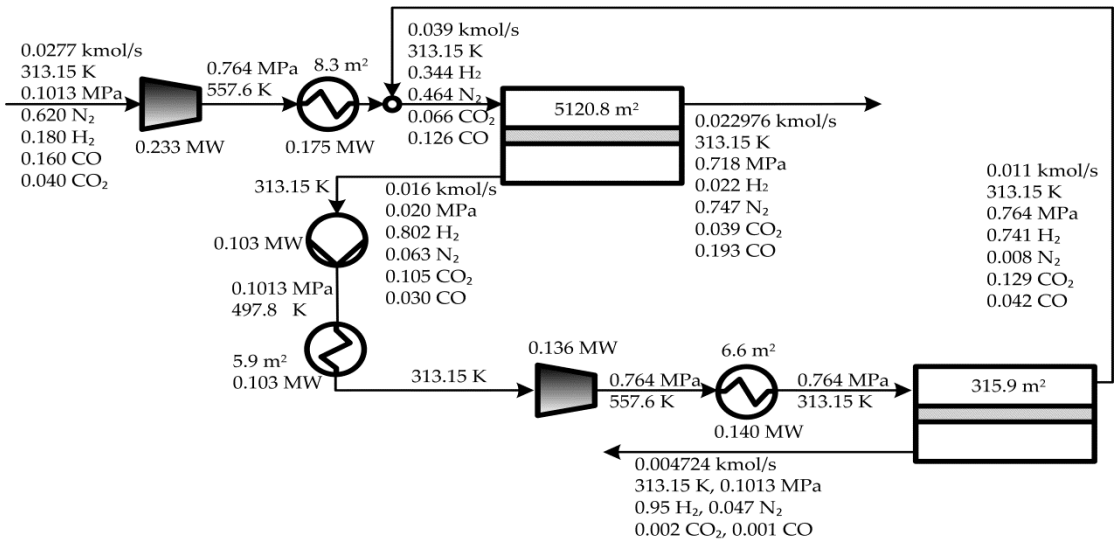

Figure 6. TAC minimization. Optimal solution for a H_2 product purity of 0.95 and H_2 recovery of 90%

However, the comparison of Figs. 4 and 6 shows that a different trade-off is established between the required total electric power and total membrane area when the H_2 product purity is increased from 0.94 to 0.95. In this case, it is necessary to increase both the total membrane area about 67.0 m² −from 5369.7 to 5436.7 m²− and the electric power about 0.065 MW −from 0.406 to 0.471 MW− in order to satisfy a desired H_2 purity of 0.95. It is interesting to note that the increase of the total membrane area results from an increase of the area of the first stage in 115.2 m² and a decrease of the area of the second stage in 48.2 m², which is a trend opposite to the one observed when the H_2 purity increases from 0.90 to 0.94 (Figs. 3 and 4), where the area of MS1 and MS2 decreases and increases, respectively, with increasing purity levels. This behavior can be better understood by observing in Fig 7 the individual variation of the area of both membranes with increasing product purity levels. The figure interestingly shows that the curve of the membrane area corresponding to MS1 has a minimum value at a H_2 purity value of 0.93, and that the one corresponding to MS2 decreases practically linearly in the studied purity variation range. This is one of the reasons of why dissimilar trade-offs between the same process variables are established at different values of H_2 purity levels.

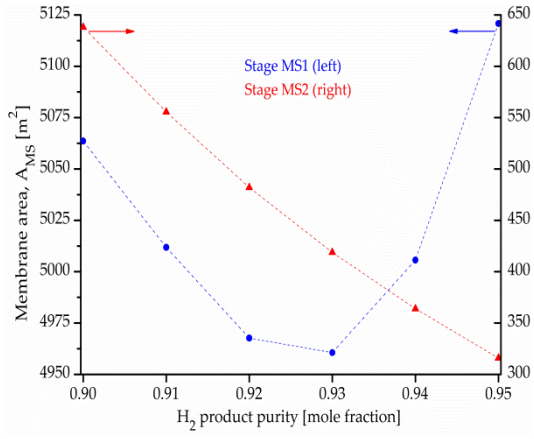

Figure 7. TAC minimization. Optimal membrane areas of stages MS1 and MS2 versus H_2 product purity.

These results clearly show the advantages of having an optimization mathematical model, mainly when both high recovery and purity levels are simultaneously targeted using membranes in gas separation processes. Certainly, it allows to identify the critical trade-offs that are otherwise difficult to distinguish at first glance.

Regarding the optimal contribution of each process unit to the total investment, Fig. 8a shows that the compressor C1 used for compressing the feed in the first stage is the largest contributor; its contribution increases practically linearly with increasing H_2 product purity values. It is followed by the compressor C2 used in the second stage for compressing the permeate leaving the vacuum pump VP1. In contrast to C1, the contribution of C2 increases exponentially with increasing H_2 product purity values, showing a behavior similar to the one observed for the optimal high operating pressure P^H values (Fig. 5). The third contributor to the total investment is the membrane area required in the first stage A_{MS1}, with an investment that remains almost constant with increasing H_2 product purities. The vacuum pump VP1 is the fourth contributor, whose investment increases more importantly at high H_2 purity values. The contributions of the remaining process units are comparatively less important or practically insignificant.

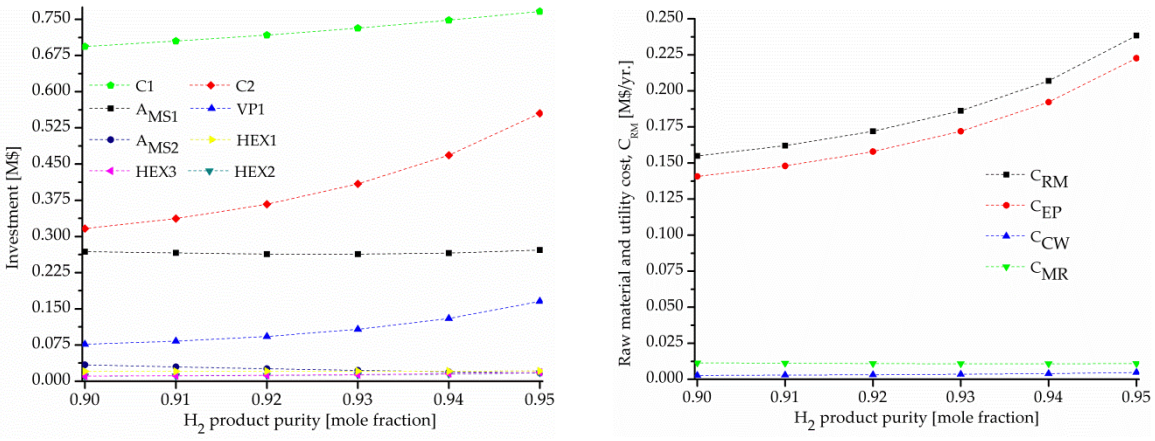

(**a**) (**b**)

Figure 8. TAC minimization. Optimal costs vs. H_2 product purity for a H_2 recovery of 90%: (**a**) Process-unit investments; (**b**) Raw material and utility cost C_{RM}, with cost for electric power EP, cooling water CW, and membrane replacement MR.

Regarding the distribution of raw material and utility cost C_{RM} shown in Fig. 8b, the cost of electricity for running the compressors and the vacuum pump is by far the major contributor, and it increases more rapidly with increasing H_2 product purity levels.

Figure 9 clearly shows that the increases in electric power required by the compressor of the second stage C2 and the vacuum pump VP1 are more significant than the increase in electric power required by compressor C1 in the first stage.

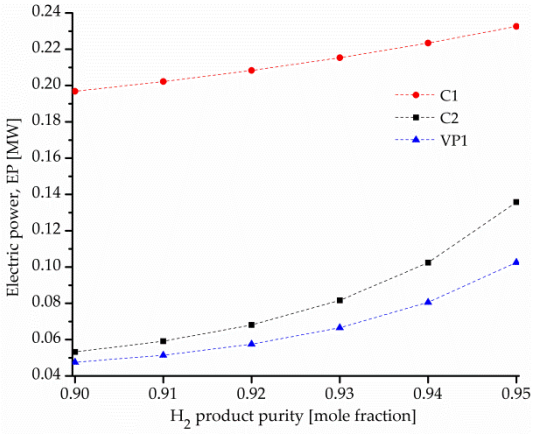

Figure 9. TAC minimization. Optimal sizes of the main process units versus H_2 product purity: (**a**) Compressors and vacuum pump; (**b**) Membrane areas of stages MS1 and MS2.

Finally, Fig. 10 shows the heat transfer areas of HEX2 and HEX3 (Fig. 10a) and their corresponding heat loads (Fig. 10b) increase in greater proportion than the ones corresponding to HEX1 with increasing H_2 purity levels. The area increases in HEX1 and HEX3 are mainly due to the increase in the compression ratio of the compressors which rises their outlet temperatures, thus requiring more area for heat transfer to reach the operating temperature of the stages (313.15 K). On the other hand, the increase of the heat transfer area of HEX2 −located after the vacuum pump VP1− and its corresponding heat load is only due to the increase in the permeate flow rate since the first stage operates with a vacuum level of 0.020 MPa, what implies the same pressure ratio (5.065) and, therefore, the same output temperature (497.8 K) for all the H_2 product purity levels.

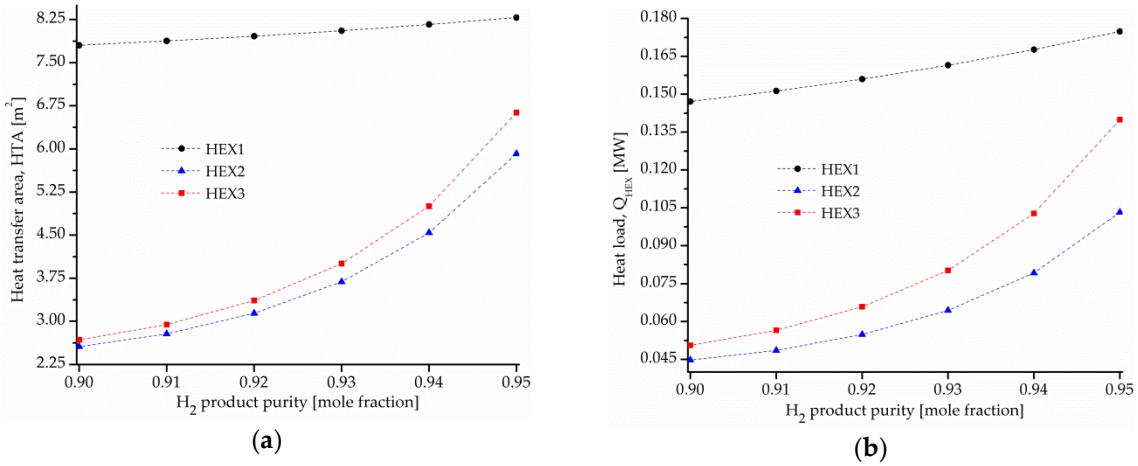

Figure 10. TAC minimization. Optimization results for heat exchangers: (**a**) Heat transfer areas and (**b**) heat loads, versus H_2 product purity.

311 *5.2. Influence of the objective functions on the optimal design and operating conditions*

312 As introduced earlier, the aim of this section is to study the influence of the objective functions
313 that are minimized on the optimal solutions and to see how these solutions can be properly used in
314 global optimization algorithms. To this end, the same process and cost mathematical models are
315 used to solve the optimization problems that result by considering the two remaining objective
316 functions: minimization of the total membrane area TMA (Eq. A32) and minimization of the total
317 power TW (Eq. A34). The optimization results obtained for the three objective functions are
318 compared in Table 2 −in terms of costs− and Table 3 −in terms of process-unit sizes and operating
319 conditions−. The optimal solutions resulting from the minimization of TAC, minimization of TMA,
320 and minimization of TW are hereafter referred as `osTAC′, `osTMA′, and `osTW′, respectively.

321 **Table 2**. Minimization of TAC, TMA, and TW for 90% H_2 recovery and 0.90 H_2 product purity: Costs

Cost item	Min TMA osTMA	Min. TAC osTAC	Min TW osTW
TAC (M$ yr^{-1})	1.85056	**1.76421**	2.11552
OPEX (M$ $yr.^{-1}$)	1.15843	1.09542	1.26216
annCAPEX (M$ $yr.^{-1}$)	0.69214	0.66879	0.85336
C_{INV} (M$)	1.48076	1.43082	1.82568
I_{C1}	0.85171	0.69360	0.48869
I_{C2}	0.36483	0.31653	0.27448
I_{MA_MS1}	0.13376	0.26859	0.83129
I_{VP1}	0.06926	0.07670	0.10428
I_{HEX1}	0.02188	0.02031	0.01799
I_{MA_MS2}	0.01843	0.03398	0.08489
I_{HEX3}	0.01101	0.01069	0.01144
I_{HEX2}	0.00987	0.01041	0.01261
C_{RM} (M$ $yr.^{-1}$)	0.19269	0.15497	0.13906
C_E	0.18332	0.14077	0.10236
C_{MR}	0.00571	0.01140	0.03463
C_{CW}	0.00366	0.00279	0.00206

322 **Table 3**. Minimization of TAC, TMA, and TW for 90% H_2 recovery and 0.90 H_2 product purity:
323 Process-unit sizes and operating conditions.

Cost item	Min TMA osTMA	Min. TAC osTAC	Min TW osTW
TMA (m^2)	**2854.23**	5701.66	17316.96
MA_{MS1}	2510.80	5063.60	15714.90
MA_{MS2}	343.43	638.06	1602.06
TW (MW)	0.38754	0.29759	**0.21639**
W_{C1}	0.27717	0.19684	0.10981
W_{C2}	0.06746	0.05325	0.04199
W_{VP1}	0.04290	0.04751	0.06459
HTA_{HEX1} (m^2)	8.83941	7.80177	6.37764
HTA_{HEX2} (m^2)	2.305	2.6	3.5

HTA_{HEX3} (m^2)	2.81339	2.68000	2.99720
Q_{HEX1} (MW)	0.20996	0.14713	0.08090
Q_{HEX2} (MW)	0.041	0.045	0.060
Q_{HEX3} (MW)	0.06682	0.05054	0.03802
ΔTML_{HEX1} (K)	85.533	67.908	45.676
ΔTML_{HEX2} (K)	62.871	62.871	61.236
ΔTML_{HEX3} (K)	85.533	67.908	45.676
P^H (MPa)	1.01320	0.59834	0.30396
P^L_{MS1} (MPa)	0.02000	0.02000	0.02102
P^L_{MS2} (MPa)	0.10132	0.10132	0.10132

Table 2 shows that the TAC value obtained in osTAC is 4.7% and 16.6% lower than those obtained in osTMA and osTW, respectively; while the OPEX value obtained in osTAC is 5.4% and 13.2% lower than the respective ones obtained in osTMA and osTW. The annCAPEX value obtained in osTAC is 3.4% and 21.6% lower than the obtained in osTMA and osTW, respectively. Table 3 shows that the minimal TMA value required by the process in solution osTMA is 2854.23 m^2, which is, respectively, 49.9% and 83.5% lower than the value obtained in osTAC and osTW, but the electric power required in osTMA is 30.2% and 79.1% higher than the required in osTAC and osTW, respectively. Table 3 shows that the minimization of TMA (2854.23 m^2) implies the highest TW value (0.38754 MW) reaching the upper bound for P^H (1.01320 MPa). Also, Table 3 shows that the minimization of TW (0.21639 MW) implies the highest TMA value (17316.96 m^2).

So far, the optimal solutions obtained by minimization of three different objective functions by using a local search algorithm have been presented. Next, the features of these solutions are considered to propose a systematic strategy for providing bounds for model variables in global optimization (GO) methods. The application of GO algorithms using deterministic mathematical models allows to obtain a solution for a given global optimality tolerance. As is well known from a computational point of view, the calculation of good lower and upper bounds is crucial for the success of any GO algorithm [16]. Sherali et al. [17] proposed an improved method to develop tight linear relaxations to calculate global lower bounds for a design problem associated with the water distribution network. To this end, they exploited the characteristics (nature) of the nonlinear constraints such as monotonicity and the convex-concave functions. The proposed method allowed to obtain novel network designs as well as to identify promising search sub-regions. Ruiz and Grossmann [18] proposed an efficient procedure to find strong bounds in generalized disjunctive (GDP) problems. Based on the theory associated with disjunctive programming, they proposed several rules to generate more efficiently new relaxations to predict strong bounds for the global optimum. The proposed procedure considerably enhanced the computational cost because it leads to a significant reduction of the number of nodes to evaluate by the branch-and-bound methods. Kirst et al. [19] presented a comprehensive discussion about the difficulties to determine good bounds in branch-and-bound methods for GO of mathematical models involving non-convex constraints. Also, they proposed a consistent way to calculate bounds by perturbing infeasible points to feasible ones by iterating along Mangasarian-Fromovitz directions. The perturbations were done using optimal solutions obtained from linear optimization problems.

Taking into consideration the above comments and the characteristics of the optimal solutions reported in Tables 2 and 3, it is interesting to investigate how the information provided by the optimal solutions corresponding to the minimization of the total membrane area (osTMA) and the total power (osTW) can be used in GO algorithms to solve the problem of minimization of the total annual cost, and therefore, to guarantee the optimality of the optimal solutions for the two-stage membrane process for H_2 separation studied in this paper −which in fact can be straightforward applied to other processes−. More precisely, in order to determine tight variable bounds, the idea behind is to use the information predicted by the same model of the process but considering two

different situations: membrane area minimization and power minimization, which represent two extremes that can be used efficiently to narrow the feasible region of the cost optimization problem. Unlike other works, it is here intended to establish a systematic bounding procedure using information inherent to the process obtained in a rational way instead of exploiting the nature of the associated constraints −at the beginning of the methodology− without applying any rational criterion.

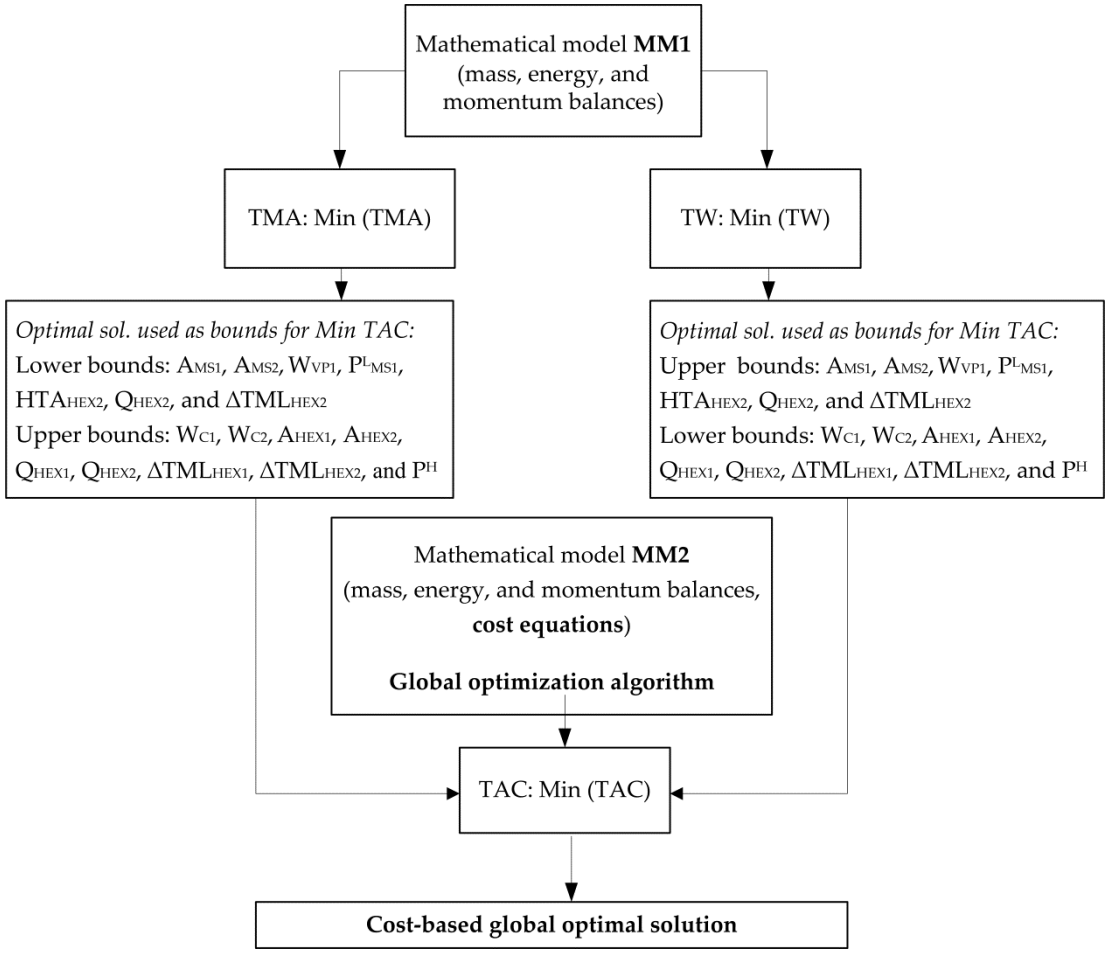

Figure 11. Schematic of a variable bounding and solution strategy proposed for solving the cost optimization problem via global optimization.

By comparing numerically the results presented in Tables 2 and 3, it can be observed that the optimal values corresponding to osTMA and osTW provide `good' lower/upper bounds for decision variables to obtain the solution osTAC to global optimality. Thus, it is possible to propose a `pre-processing' phase to systematically and rationally provide good lower and upper bounds to solve the cost minimization problem to global optimality. The schematic of the proposed pre-processing methodology (Fig. 11) shows that two optimization problems −which only differ on the objective function− are solved by using a same mathematical model of the process without including cost constraints (model MM1). The first step is to solve the minimization of TMA; the optimal values of A_{MS1}, A_{MS2}, W_{VP1}, P^{L}_{MS1}, HTA_{HEX2}, Q_{HEX2}, and ΔTML_{HEX2} are provided as lower bounds to solve the minimization of TAC while the optimal values of W_{C1}, W_{C2}, A_{HEX1}, A_{HEX2}, Q_{HEX1}, Q_{HEX2}, ΔTML_{HEX1}, ΔTML_{HEX2}, and P^{H} are provided as upper bounds. The second step consists on the minimization of TW; the optimal values of W_{C1}, W_{C2}, A_{HEX1}, A_{HEX2}, Q_{HEX1}, Q_{HEX2}, ΔTML_{HEX1}, ΔTML_{HEX2}, and P^{H} are now provided as lower bounds while the values of A_{MS1}, A_{MS2}, W_{VP1}, P^{L}_{MS1}, HTA_{HEX2}, Q_{HEX2}, and ΔTML_{HEX2} as upper bounds. Thus, if the minimization of TMA provides a lower bound for a given decision variable, then the minimization of TW provides an upper bound for it, and vice versa. It is said that the pre-processing phase provides bounds in a rational way because they represent

limits for the sizes of the pieces of equipment and/or process operation conditions. They can be used to identify smaller search spaces for the cost optimization problem and reduce the number of iterations, and consequently, the computing time. In addition, one of the two solutions (osTMA or osTW) can be used as an initial guess point in the global optimization algorithm because they are both feasible solutions for the cost optimization problem, thus facilitating the model convergence.

6. Conclusions

This paper presented the optimization results of a two-stage membrane system for H_2 separation by minimization of the total annual cost, the total membrane area, and the total electric power as single objective functions, employing a nonlinear mathematical model implemented in GAMS environment.

First, a detailed discussion of optimal solutions obtained by minimizing the total annual cost for desired H_2 product purity values ranging between 0.90 and 0.95 and keeping constant the H_2 recovery at 90% was presented. One of the optimization results showed that an increment of H_2 product purity in 0.01 determines different percentage variations in costs depending on the purity level itself. For instance, an increment of H_2 purity from 0.90 to 0.91 implies an increase of the total annual cost in 0.03739 M$ $yr.^{-1}$ (2.1%) while the same increment from 0.94 to 0.95 implies an increase in 0.17274 M$ $yr.^{-1}$ (8.4%). Also, the optimal trade-off existing between the total membrane area and the total electric power depends on the values of H_2 purity. In fact, it was found that different trade-offs are established between the required total electric power and the total membrane area when the H_2 product purity is increased from 0.90 to 0.94 and from 0.94 to 0.95. In the former case, the total electric power increases and the total membrane area decreases with the increasing of the H_2 purity. The optimal cost-based trade-offs indicated that it is more beneficial to increase the total electric power −to operate the process at higher operating pressure values− rather than to increase the total membrane area. However, in the last case, it was observed that both the total membrane area and the total electric power increase with the increasing of the H_2 product purity.

The proposed mathematical model was solved considering the three aforementioned objective functions, and the obtained solutions were compared. From this comparison, it was observed that the optimal values obtained by minimizing the total membrane area and the total electric power −as single objectives− are `good' bounds when the total annual cost is intended to be minimized to global optimality. By inspecting the numerical value of each model variable and the objective function, it is possible to propose a `pre-processing' phase to systematically and rationally provide good lower and upper bounds to solve the minimization of the total annual cost to global optimality. In this work, a local search optimization algorithm was used for cost minimization. In a next paper, a global optimization algorithm will be used instead, exploiting these solution features.

Author Contributions: All authors contributed to the analysis of the results and to writing the manuscript. A.M.A and P.L.M developed and implemented in GAMS the generic mathematical model of a membrane module and the cost model, and collected and analyzed data. S.F.M. developed and implemented in GAMS the model of the whole process, and wrote the first draft of the manuscript. N.J.S improved the discussion of results. J.A.C contributed with numerical and solution issues. M.C.M. conceived and supervised the research and provided feedback to the content.

Acknowledgments: The financial support from the Consejo Nacional de Investigaciones Científicas y Técnicas (CONICET), the Agencia Nacional de Promoción Científica y Tecnológica (ANPCyT), and the Facultad Regional Rosario of the Universidad Tecnológica Nacional (UTN) from Argentina is gratefully acknowledged.

Conflicts of Interest: The authors declare no conflict of interest.

Appendix A: Process mathematical model

A.1. Main model assumptions

The assumptions considered for modeling the membrane units are [8]:

- All components can permeate.

- The component permeability is not affected by the operating pressure.
- The pressure drop is negligible at both membrane sides.
- The pressure of the feed and retentate streams is the same.
- Plug-flow pattern is considered at both membrane sides.
- Each membrane module operates isothermally.
- The Fick's first law is used.

A.2. Mathematical model

A.2.1. Mass balances

Figure A1a and A1b schematize the process configuration and the membrane module, respectively, that are modeled. The equations describing the mass balance of component i in the membrane module MS1, by applying the backward finite difference discretization method, are:

$$\frac{1}{2}\frac{(J-1)}{A_{MS1}}\left(-F_{MS1,j}\cdot x_{MS1,i,j}+F_{MS1,j+2}\cdot x_{MS1,i,j+2}\right)+\xi_i\left(P^H\cdot x_{MS1,i,j+1}-P^L_{MS1}\cdot y_{MS1,i,j+1}\right)=0;\ \ j=0,\ \forall i \quad (A1)$$

$$\begin{aligned}&\frac{1}{2}\frac{(J-1)}{A_{MS1}}\cdot\left(F_{MS1,j}\cdot x_{MS1,i,j}-4\cdot F_{MS1,j+1}\cdot x_{MS1,i,j+1}+3\cdot F_{MS1,j+2}\cdot x_{MS1,i,j+2}\right)+\\&\xi_i\cdot\left(P^H\cdot x_{MS1,i,j+2}-P^L_{MS1}\cdot y_{MS1,i,j+2}\right)=0;\ \ j=0,\ldots,J-2\end{aligned} \quad (A2)$$

ξ_i and A_{MS1} are the permeance of component i and membrane surface area, respectively. P^H and $P^L{}_{MS1}$ are the operating pressures in the retentate and permeate sides, respectively. The index j refers to a discretization point which varies from 0 to 19 (J=19, i.e. 20 discretization points is considered).

$$F_{MS1,j=0}\cdot x_{MS1,i,j=0}-F_{MS1,j=J}\cdot x_{MS1,i,j=J}-P_{MS1,j=0}\cdot y_{MS1,i,j=0}=0;\ \forall i \quad (A3)$$

$$F_{MS1,j=0}-F_{MS1,j=J}-P_{MS1,j=0}=0 \quad (A4)$$

$$\sum_i x_{MS1,i,j}=1;\ \ \forall j,\ i=H_2, N_2, CO_2, CO \quad (A5)$$

$$\sum_i y_{MS1,i,j}=1;\ \ \forall j,\ i=H_2, N_2, CO_2, CO \quad (A6)$$

The second membrane stage MS2 is modeled in a similar way.

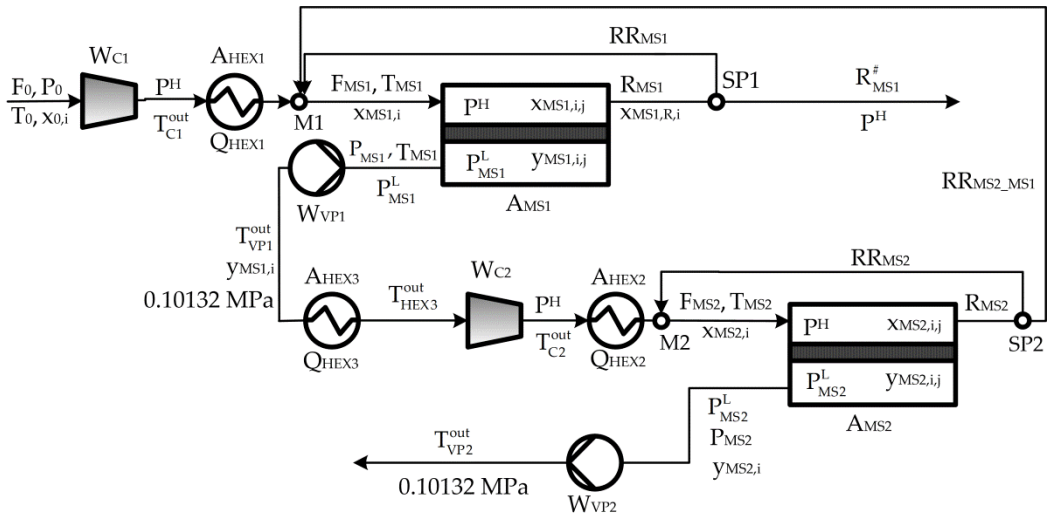

(**a**)

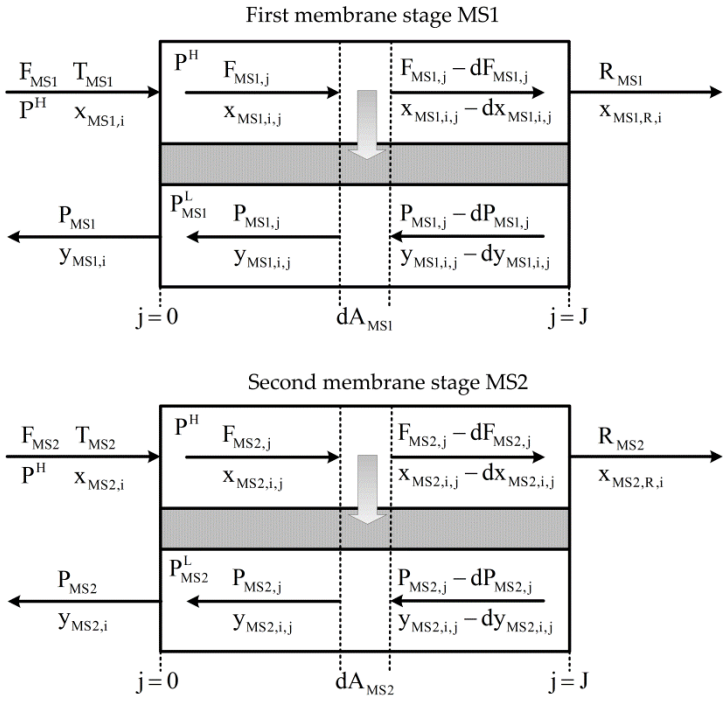

(**b**)

Figure A1. Representation and nomenclature: (**a**) Whole process; (**b**) Membrane modules.

The mass balances in splitters SP1 and SP2 are:

$$R_{MS1} = RR_{MS1} + R^{\#}_{MS1} \tag{A7}$$

$$R_{MS2} = RR_{MS2} + RR_{MS2\_MS1} \tag{A8}$$

A.2.2. Power requirement

The electric power required by compressors (C1, C2) and vacuum pumps (VP1, VP2) are calculated as follows:

$$W_{C1} = \frac{F_0}{\eta_C} \cdot \left(\frac{\gamma}{\gamma - 1}\right) \cdot R \cdot T_0 \cdot \left[\left(\frac{P^H}{P_0}\right)^{\frac{\gamma-1}{\gamma}} - 1\right] \tag{A9}$$

$$\frac{T^{out}_{C1}}{T_0} = \left(\frac{P^H}{P_0}\right)^{\frac{\gamma-1}{\gamma}} \tag{A10}$$

$$W_{C2} = \frac{P_{MS1}}{\eta_C} \cdot \left(\frac{\gamma}{\gamma - 1}\right) \cdot R \cdot T^{out}_{HEX3} \cdot \left[\left(\frac{P^H}{P_0}\right)^{\frac{\gamma-1}{\gamma}} - 1\right] \tag{A11}$$

$$\frac{T^{out}_{C2}}{T^{out}_{HEX3}} = \left(\frac{P^H}{P_0}\right)^{\frac{\gamma-1}{\gamma}} \tag{A12}$$

γ, η_c, and P_0 are the adiabatic expansion coefficient (1.4), efficiency (0.85), and atmospheric pressure (0.1013 MPa), respectively.

$$W_{VP1} = \frac{P_{MS1}}{\eta_C} \cdot \left(\frac{\gamma}{\gamma - 1} \right) \cdot R \cdot T_{MS1} \cdot \left[\left(\frac{P_0}{P_{MS1}^L} \right)^{\frac{\gamma-1}{\gamma}} - 1 \right] \tag{A13}$$

$$\frac{T_{VP1}^{out}}{T_{MS1}} = \left(\frac{P_0}{P_{MS1}^L} \right)^{\frac{\gamma-1}{\gamma}} \tag{A14}$$

$$W_{VP2} = \frac{P_{MS2}}{\eta_C} \cdot \left(\frac{\gamma}{\gamma - 1} \right) \cdot R \cdot T_{MS2} \cdot \left[\left(\frac{P_0}{P_{MS2}^L} \right)^{\frac{\gamma-1}{\gamma}} - 1 \right] \tag{A15}$$

$$\frac{T_{VP2}^{out}}{T_{MS2}} = \left(\frac{P_0}{P_{MS2}^L} \right)^{\frac{\gamma-1}{\gamma}} \tag{A16}$$

A.2.3. Energy balances and transfer areas of heat exchangers

The energy balances in the heat exchangers and their heat transfer areas are calculated by Eqs. (A17−A25):

$$F_0 \cdot c_P^g \cdot \left(T_{C1}^{out} - T_{MS1} \right) = n_{HEX1,cw} \cdot c_P^{cw} \cdot \left(T_{HEX1,cw}^{out} - T_{HEX1,cw}^{inl} \right) \tag{A17}$$

$$P_{MS1} \cdot c_P^g \cdot \left(T_{C2}^{out} - T_{MS2} \right) = n_{HEX2,cw} \cdot c_P^{cw} \cdot \left(T_{HEX2,cw}^{out} - T_{HEX2,cw}^{inl} \right) \tag{A18}$$

$$P_{MS1} \cdot c_P^g \cdot \left(T_{VP1}^{out} - T_{HEX3}^{out} \right) = n_{HEX3,cw} \cdot c_P^{cw} \cdot \left(T_{HEX3,cw}^{out} - T_{HEX3,cw}^{inl} \right) \tag{A19}$$

$$A_{HEX1} = \frac{F_0 \cdot c_P^g \cdot \left(T_{C1}^{out} - T_{MS1} \right)}{U \cdot LMTD_{HEX1}} \tag{A20}$$

$$A_{HEX2} = \frac{P_{MS1} \cdot c_P^g \cdot \left(T_{C2}^{out} - T_{MS2} \right)}{U \cdot LMTD_{HEX2}} \tag{A21}$$

$$A_{HEX3} = \frac{P_{MS1} \cdot c_P^g \cdot \left(T_{VP1}^{out} - T_{HEX3}^{out} \right)}{U \cdot LMTD_{HEX3}} \tag{A22}$$

$$LMTD_{HEX1} = \frac{\left(T_{C1}^{out} - T_{HEX1,cw}^{out} \right) - \left(T_{MS1} - T_{HEX1,cw}^{inl} \right)}{\ln \frac{\left(T_{C1}^{out} - T_{HEX1,cw}^{out} \right)}{\left(T_{MS1} - T_{HEX1,cw}^{inl} \right)}} \tag{A23}$$

$$LMTD_{HEX2} = \frac{\left(T_{C2}^{out} - T_{HEX2,cw}^{out} \right) - \left(T_{MS2} - T_{HEX2,cw}^{inl} \right)}{\ln \frac{\left(T_{C2}^{out} - T_{HEX2,cw}^{out} \right)}{\left(T_{MS2} - T_{HEX2,cw}^{inl} \right)}} \tag{A24}$$

$$LMTD_{HEX3} = \frac{\left(T_{VP1}^{out} - T_{HEX3,cw}^{out}\right) - \left(T_{HEX3}^{out} - T_{HEX3,cw}^{inl}\right)}{\ln \frac{\left(T_{VP1}^{out} - T_{HEX3,cw}^{out}\right)}{\left(T_{HEX3}^{out} - T_{HEX3,cw}^{inl}\right)}} \quad (A25)$$

The parameter U is the overall heat transfer coefficient, which is assumed to be 277.7 10^{-4} MW dam^{-2} K^{-1} for all heat exchangers.

A.2.4. Connecting constraints

The constraints used to relate model variables defined inside and outside of the membrane module MS1 are:

$$F_{MS1} = F_{MS1,j=0} \quad (A26)$$

$$x_{MS1,i} = x_{MS1,i,j=0} \quad (A27)$$

$$F_{MS1,j=J} = R_{MS1} \quad (A28)$$

$$x_{MS1,i,j=J} = x_{MS1,R,i} \quad (A29)$$

$$P_{MS1} = P_{MS1,j=0} \quad (A30)$$

$$y_{MS1,i} = y_{MS1,i,j=0} \quad (A31)$$

Similar constraints are necessary for the membrane stage MS2.

A.2.5. Performance variables

The total membrane area TMA, total heat transfer area THTA, and total power are calculated by Eqs. (A32−A34), respectively:

$$TMA = A_{MS1} + A_{MS2} \quad (A32)$$

$$THTA = A_{HEX1} + A_{HEX2} + A_{HEX3} + A_{HEX4} \quad (A33)$$

$$TW = W_{C1} + W_{C2} + W_{VP1} + W_{VP2} \quad (A34)$$

Nomenclature

$A_{MS\#}$: membrane area required in the membrane stage MS#, m^2.
annCAPEX: annualized capital expenditures, M$ $yr.^{-1}$
CAPEX: capital expenditures, M$.
CRF: capital recovery factor, $yr.^{-1}$
C_{RM}: raw material and utility cost, M$ $yr.^{-1}$
cru_{CW}: specific cost of the cooling water, M$ kg^{-1}.
cru_{EE}: specific cost of the electricity, M$ kW^{-1}.
cru_{MR}: specific cost of the membrane replacement, M$ m^{-2}.
F_0: feed flow rate, kmol s^{-1}.
$F_{MS\#}$: feed flow rate in the membrane stage MS#, kmol s^{-1}.
$I_{MS\#}$: investment for membrane area of the stage MS#, M$.

$I_{HEX\#}$: investment for the heat exchanger HEX#, M$.

$I_{VP\#}$: investment for the vacuum pump VP#, M$.

$I_{C\#}$: investment for the compressor C#, M$.

OPEX: operating expenditures, M$ $yr.^{-1}$

P^{H}: high operating pressure (retentate side), MPa.

$P_{MS\#}$: permeate flow rate obtained in the membrane stage MS#, kmol s^{-1}.

$P^{L}_{MS\#}$: operating pressure in the permeate side of the membrane stage MS#, MPa.

$R_{MS\#}$: retentate flow rate obtained in the membrane stage MS#, kmol s^{-1}.

TAC: total annual cost, M$ $yr.^{-1}$

T_0: feed temperature, K.

$T^{out}{}_{C\#}$: outlet temperature from the compressor C# associated with the membrane stage MS#, K.

$T_{MS\#}$: operating temperature in the membrane stage MS#, K.

$T^{out}{}_{HEX\#}$: outlet temperature from the heat exchanger HEX#, K.

TW: total power, MW.

$W_{C\#}$: power required by the compressor C# associated with the membrane stage MS#, MW.

$W_{VP\#}$: power required by the vacuum pump VP# in the membrane stage MS#, MW.

$x_{i,0}$: mole fraction of component i in the feed stream, dimensionless.

$x_{MS\#,i}$: inlet composition of the component i in the membrane stage MS#, dimensionless.

$x_{MS\#,i,j}$: mole fraction of the component i in the retentate stream of the membrane stage MS# at the discretization point j, dimensionless.

$x_{MS\#,R,i}$: mole fraction of the component i in the retentate stream leaving the membrane stage MS#, dimensionless.

$y_{MS\#,i}$: mole fraction of the component i in the permeate stream leaving the membrane stage MS#, dimensionless.

$y_{MS1,i,j}$: mole fraction of the component i in the permeate stream of the membrane stage MS# at the discretization point j, dimensionless.

References

1. Ahmad, F.; Lau, K.K.; Shariff, A.M.; Murshid, G. Process simulation and optimal design of membrane separation system for CO_2 capture from natural gas. *Comp. Chem. Eng*. **2012**, *36*, 119-128, DOI:10.1016/j.compchemeng.2011.08.002.
2. Chowdhury, M.H.M.; Feng, X.; Douglas, P.; Croiset, E. A new numerical approach for a detailed multicomponent gas separation membrane model and AspenPlus Simulation. *Chem. Eng. Technol*. **2005**, *28* (7), 773-782, DOI:10.1002/ceat.200500077.
3. Xu, J.; Wang, Z.; Zhang, C.; Zhao,S.; Qiao, Z.; Li, P.; Wang, J.; Wang, S. Parametric analysis and potential prediction of membrane processes for hydrogen production and pre-combustion CO_2 capture. *Chem. Eng. Sci*. **2015**, *135*, 202-216, DOI:10.1016/j.ces.2015.04.033.
4. Giordano, L.; Roizard, D.; Bounaceur, R.; Favre, E. Energy penalty of a single stage gas permeation process for CO_2 capture in post-combustion: A rigorous parametric analysis of temperature, humidity and membrane performances. *Energy Procedia*, **2017**, *114*, 636-641, DOI:10.1016/j.egypro.2017.03.1206.
5. Turi, D.M.; Ho, M.; Ferrari, M. C.; Chiesa, P.; Romano, M.C. CO_2 capture from natural gas combined cycles by CO_2 selective membranes. *Int. J. Greenh. Gas Con.* **2017**, *61*, 168-183, DOI:10.1016/j.ijggc.2017.03.022.
6. Ghasemzadeh, K.; Jafari, M.; Sari, A.H.; Babalou, A.A. Performance investigation of membrane process in natural gas sweeting by membrane process: Modeling study. *Chem. Prod. Process Model*. **2016**, *11*(1), 23–27.

7. Zarca, L.; Urtiaga, A.; Biegler, L.T.; Ortiz I. An optimization model for assessment of membrane-based post-combustion gas upcycling into hydrogen or syngas. *J. Memb. Sci.* **2018**, *563*, 83-92, DOI:10.1016/j.memsci.2018.05.038.
8. Arias, A.M.; Mussati, M.C.; Mores, P.L.; Scenna, N.J., Caballero, J.A.; Mussati, S.F. Optimization of multi-stage membrane systems for CO_2 capture from flue gas. *Int. J. Greenh. Gas Control* **2016**, *53*, 371-390, DOI:10.1016/j.ijggc.2016.08.005.
9. Ramírez-Santos, A.A.; Bozorg, M.; Addis, B.; Piccialli, V.; Castel, C.; Favre, E. Optimization of multistage membrane gas separation processes. Example of application to CO_2 capture from blast furnace gas. *J. Membr.Sci.* **2018**, *566*, 346-366, DOI:10.1016/j.memsci.2018.08.024.
10. Ohs, B.; Lohaus, J.; Wessling, M. Optimization of membrane based nitrogen removal from natural gas. *J. Memb. Sci.* **2016**, *498*, 291-301, DOI:10.1016/j.memsci.2015.10.007.
11. Arias, A.M. Minimization of greenhouse gases (GHGs) emissions in the energy sector employing non-conventional technologies. PhD Thesis, Universidad Tecnológica Nacional, Argentina, 2017. (In Spanish).
12. Abu-Zahra, M.R.M.; Niederer, J.P.M.; Feron, P.H.M.; Versteeg, G.F. CO_2 capture from power plants: Part II. A parametric study of the economical performance based on mono-ethanolamine, *Int. J. Greenh. Gas Control* **2007**, 1, 135-142, DOI:10.1016/S1750-5836(07)00032-1.
13. Rao, A.B.; Rubin, E.S. A technical, economic, and environmental assessment of amine-based CO_2 capture technology for power plant greenhouse gas control. *Environ. Sci. Technol*. **2002**, 36, 4467-4475, DOI:10.1021/es0158861.
14. GAMS Development Corporation. General Algebraic Modeling System *GAMS*, Release 24.2.1. **2013**, Washington DC, USA. http://www.gams.com
15. Drud, A.S. CONOPT 3 solver manual **2012**, ARKI Consulting and Development A/S, Bagsvaerd, Denmark.
16. Puranik, Y.; Sahinidis, N.V. Domain reduction techniques for global NLP and MINLP optimization. *Constraints* **2017**, *22*(3), 338–376, DOI: 10.1007/s10601-016-9267-5.
17. Sherali, H.D.; Totlani, E.; Loganathan, G.V. Enhanced lower bounds for the global optimization of water distribution. *Water Resour. Res.* **1998**, *34* (7), 1831-1841, DOI:10.1029/98WR00907.
18. Ruiz, J.P.; Grossmann, I.E. A new theoretical result for convex nonlinear generalized disjunctive programs and its applications. *Proceedings of the 22nd European Symposium on Computer Aided Process Engineering* **2012**, 1—20, 1197-1201.
19. Kirst, P.; Stein, O.; Steuerman, P. Deterministic upper bounds for spatial branch-and-bound methods in global minimization with nonconvex constraints. *TOP* **2015**, *23*(2), 591–616, DOI:10.1007/s11750-015-0387-7.